Electronic Structure Methods for Simulating Flavin's Spectroscopy and Photophysics: Comparison of Multi-Reference, Single-Reference, and TD-DFT Methods

Mohammad Pabel Kabir,[1] Paulami Ghosh,[1] Samer Gozem[1,*]

[1]Department of Chemistry, Georgia State University, Atlanta, GA 30302, United States.

Abstract

The use of flavins and flavoproteins in photocatalytic, sensing, and biotechnological applications has led to a growing interest in computationally modeling the excited state electronic structure and photophysics of flavin. However, there is limited consensus regarding which computational methods are appropriate for modeling flavin's photophysics. We compare the energies of low-lying excited states of flavin computed with time-dependent density functional theory (TD-DFT), equation of motion coupled cluster (EOM-EE-CCSD), scaled opposite-spin configuration interaction (SOS-CIS(D)), multiconfiguration pair-density functional theory (MC-PDFT), and several multi-reference perturbation theory (MR-PT2) methods. In the first part, we focus on excitation energies of the first singlet excited state (S_1) of five different redox and protonation states of flavin, with the goal of finding a suitable active space for MR-PT2 calculations. In the second part, we construct two sets of one-dimensional potential energy surfaces connecting the S_0 and S_1 equilibrium geometries (S_0–S_1 path) and the S_1 (π,π^*) and S_2 (n,π^*) equilibrium geometries (S_1–S_2 path). The first path therefore follows a Franck-Condon active mode of flavin while the second path maps crossings points between low-lying singlet and triplet states in flavin. We discuss the similarities and differences in the TD-DFT, EOM-EE-CCSD, SOS-CIS(D), MC-PDFT and MR-PT2 energy profiles along these paths. We find that (TD-)DFT methods are suitable for applications such as simulating the spectra of

flavins but are inconsistent with several other methods when used for some geometry optimizations and when describing the energetics of dark (n,π*) states. MR-PT2 methods show promise for the simulation of flavin's low-lying excited states, but the selection of orbitals for the active space and in the number of roots used for state averaging must be done carefully to avoid artefacts. Some properties, such as the intersystem crossing geometry and energy between the S_1 (π,π*) and T_2 (n,π*) states, may require additional benchmarking before they can be determined quantitatively.

Introduction

Flavins are cofactors in several classes of enzymes and in photoreceptor proteins, where they are typically bound as either flavin mononucleotide (FMN) or flavin adenine dinucleotide (FAD). Flavins are often encountered in one of three redox states: the oxidized quinone (Fl), the one-electron reduced radical semiquinone ($FlH^{\bullet}$), and the two-electron fully reduced hydroquinone (FlH_2). The pKa values of these states are 10.3, 8.3, and 6.7 in aqueous solutions, respectively.[1-3] Therefore, the semiquinone and hydroquinone redox states are frequently also encountered in their deprotonated anionic forms, $Fl^{\bullet-}$ and FlH^{-}, under physiological conditions (Scheme 1). These redox and protonation states play an important role in either coupled or stepwise electron and/or proton transfer reactions (**Fig. 1**). Here, we refer collectively to FMN, FAD, riboflavin, and lumiflavin (LF) as flavins, since they all share the same tricyclic 7,8-dimethyl alloxazine group.

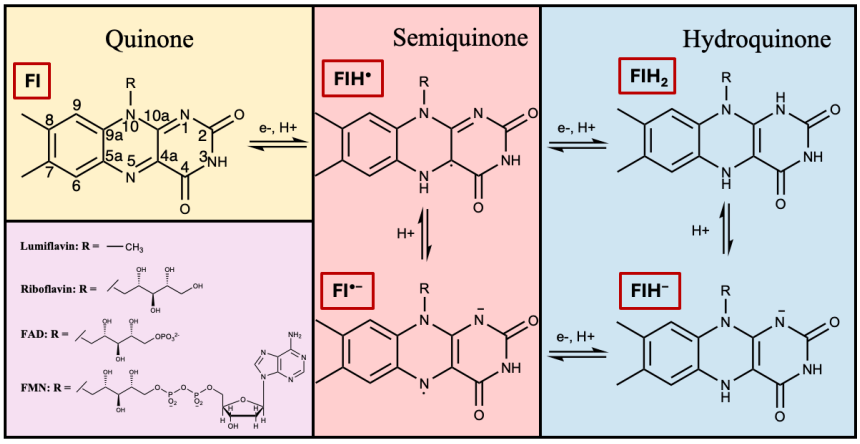

Figure 1: Structure of flavins in different redox and protonation states. The atom numbering is shown for the quinone (Fl) structure.

Flavin cofactors catalyze an impressive range of chemical transformations in different enzymes and are involved in several primary and secondary metabolic pathways.[4-7] Flavoproteins are critical to all the main energy generation metabolisms[8] including

photosynthesis,[9] aerobic and anaerobic respiration,[10-12] and denitrification.[13, 14] Flavins also serve as chromophores in several photoreceptors and light-responsive enzymes including cryptochromes,[15] LOV domains (phototropins),[16] BLUF,[17] and DNA photolyases.[18, 19]

In its oxidized form, flavin has two absorption bands in the near-UV and visible range, one band centered around 450 nm, associated with excitation to the first singlet excited state ($\mathbf{S_1}$), and a second band at around 380 nm associated with excitation to a higher singlet excited state. These absorption wavelengths are relatively insensitive to the solvent or protein environment.[20, 21] Both of those states have π,π* excitation character. Other low-lying excited states also exist in that energy range, including triplet states and singlet states, but those states have substantially smaller oscillator strengths (extinction coefficients) and do not appear in the UV/visible spectrum. Even though such dark states do not get directly excited, they can play an important role in flavins' photophysics, as exemplified by LOV domains that undergo intersystem crossing (ISC) followed by adduct formation.[22, 23]

Blue light absorption excites flavin to its S_1 state. Higher energy (near-UV or UV) absorption also ultimately populates the same state after a series of internal conversions and vibrational relaxations, per Kasha's rule.[24] Therefore, flavin's S_1 state often acts as the launch pad for flavin's further photophysics. From there, flavin may undergo fluorescence,[25-27] ISC to a triplet state,[25, 28] electron transfer,[29] or photochemical reactions, forming adducts and derivatives with neighboring amino acids.[23, 30-32] These photophysical properties have been harnessed in applications including biosensing, bioimaging, optogenetics, singlet oxygen generation, and FRET spectroscopy.[25, 28, 33-35]

Unlike the π,π* transitions responsible for flavins' two UV/vis absorption bands, the energies of flavin's low-lying dark states, especially those having n,π* character, can be sensitive

to interactions with a solvent or protein.[21, 36, 37] Since those states are relevant to flavin's photophysics, computational modeling can be a powerful tool to study their energetics in different protein environments. However, most computational studies on flavins have focused on their ground state or on bright excited states. Several studies have shown that time-dependent density functional theory (TD-DFT) is suitable for simulating flavin's UV-visible spectra when accounting for Franck-Condon factors.[21, 37-39] On the other hand, TD-DFT has not been as thoroughly tested for describing excited states relevant to flavin's photophysics, including triplet, n,π*, or redox states.

When dealing with a manifold of excited states with degenerate or nearly degenerate orbitals or states, multi-configurational wave function methods such as complete active-space self-consistent field (CASSCF)[40] are suitable. In CASSCF, a full configuration interaction is carried out for select electrons and orbitals (the active space). While CASSCF misses dynamical electron correlation for electrons outside of the active space, post-CASSCF (multi-reference) methods can be used to correct for this missing correlation. Second-order multi-reference perturbation (MR-PT2) theories such as single state (SS-)CASPT2 and multi-state (MS-)CASPT2 are widely used.[41, 42] More recently, to address issues with artefacts in SS-CASPT2 and MS-CASPT2 arising at near-degeneracies of the underlying CASSCF reference wave function, methods like the extended multi-state (XMS) CASPT2[43] and Extended Dynamically Weighted (XDW) CASPT2[44] have been developed. The former employs a treatment of the zeroth order Hamiltonian proposed as by Granovsky[45] which removes the artefacts but alters the energy of the states of interest compared to MS-CASPT2. The latter approach, XDW-CASPT2, also addresses the artefacts but largely preserves the energies of the MS-CASPT2 states.

An alternative approach for accounting for static and dynamical electron correlation is the multiconfiguration pair-density functional theory (MC-PDFT),[46, 47] which combines favorable characteristics of CASSCF and DFT. MC-PDFT is another approach that has found a range of applications from transition metal chemistry to mechanistic studies on biological photoreceptors.[48, 49]

Several methods, including semi-empirical, TD-DFT, and multi-reference (often, MR-PT2) methods have been used already to calculate the excited state properties of flavins.[21, 36-39, 50-81] For multi-reference calculations, the issue of active space selection is a recurring theme and a decision is often made that balances computational cost and computational accuracy due to the steep increase in computational cost with the size of the active space. Automated protocols to select the active space have been developed by several research groups.[74, 82-86] Sayfutyarova and Hammes-Schiffer applied their automated protocol that is based on Hückel theory for the selection of a suitable active space for flavin's π-conjugated orbitals.[74] However, the choice of active space is also dependent on the problems and states of interest. For example, for calculating bright π,π* transitions, it is often adequate to include only π electrons and π and π* orbitals in the active space. For the calculation of dark n,π* states, however, including non-bonding orbitals in the active space is required. Therefore, there is still a need to tailor active spaces not only to the system but also to the problem of interest.

We present a benchmark study focused on flavin's low-lying excited states that are relevant to flavin's early photophysics. We focus on LF (**Fig. 1**), a minimal flavin model that contains the spectroscopically and photochemically relevant isoalloxazine tricyclic moiety. We test several TD-DFT, equation of motion coupled cluster (EOM-EE-CCSD),[87, 88] scaled opposite-spin configuration interaction (SOS-CIS(D)),[89] MC-PDFT, and several MR-PT2

methods. For MR-PT2, we present the effect of modifying parameters including the active spaces and state averaging. We initially focus on excitation energies to the S_1 excited state of each redox state. We then move on to potential energy scans (PESs) of low-lying excited states, tracing the coordinates from the Franck-Condon point (at the ground state optimized geometry) to the S_1 (π,π^*) minimum and then from the S_1 (π,π^*) minimum to the S_2 (n,π^*) minimum. These scans are used to probe the reliability of different methods across key geometries and state crossing points.

Computational Details

Vertical excitation calculations

Each of the five redox states of LF shown in **Fig. 1** (Fl, $FlH^{\bullet}$, $Fl^{\bullet-}$, FlH^-, FlH_2) were optimized in the gas phase using second-order Møller-Plesset perturbation theory (MP2) with the correlation-consistent polarized valence triple-ζ (cc-PVTZ) basis set. The optimizations were performed without the use of symmetry. In the case of Fl, $FlH^{\bullet}$, and $Fl^{\bullet-}$, the isoalloxazine ring remains planar during the optimization. However, FlH^- and FlH_2 are bent at the central ring at their equilibrium geometry, exhibiting what has been referred to as a butterfly bend.[21, 90-92]

Vertical excitation energies were computed using CASSCF, MC-PDFT, SS-CASPT2, MS-CASPT2, XMS-CASPT2, XDW-CASPT2. Energies were also computed using TD-DFT with the B3LYP functional, which has been shown to give adiabatic excitation energies for the oxidized form of flavin consistent with experiments.[21, 38, 39, 61] The TD-DFT calculations were carried out using cc-pVTZ, while the ANO-L-VDZP basis set was used for the CASSCF, MC-PDFT, and MR-PT2 calculations.

To determine a suitable starting point for the active space, orbital entanglement calculations were carried out at the CASSCF density matrix renormalization group (CASSCF-DMRG) level of theory[86, 93] and ANO-L-VDZP basis set. Orbital entanglement figures were generated using autoCAS,[94] and served as starting point for the selection of the active space orbitals for CASSCF and multi-reference calculations. The number of active space orbitals and electrons were gradually reduced based on their occupancy to test the effect of using a smaller active space on the excitation energies. The number of roots used in the state averaging was also benchmarked.

To mitigate the issue of intruder states in MR-PT2 calculations, an imaginary shift was used.[95] We tried using a real shift, which gave similar energies except for a few spurious spikes in the excitation energy.[96, 97] We also tested the effect of applying a shifted zeroth-order Hamiltonian (IPEA shift) utilizing the default value of 0.25 atomic units.[98] The IPEA shift is often used as an approximate correction for an unbalanced description of open-shell and closed shell electronic states, although it may not be needed if a sufficiently large basis set and active space is used.[99]

Potential energy scans (PESs)

To generate one-dimensional potential energy scans along coordinates relevant to flavin's photophysics, we reoptimized the S_0, S_1, and S_2 states of flavin at the (TD-)B3LYP/cc-pVTZ with C_s symmetry enforced. We then generated two 1-D PESs by linear interpolation of Cartesian coordinates. The first PES (S_0 – S_1 path, see **Fig. 2** left) connects the S_0 optimized geometry to the S_1 optimized geometry and therefore follows a Franck-Condon-active mode. The second PES (S_1–S_2 path, see **Fig. 2** right) connects the S_1 optimized geometry to the S_2

optimized geometry and therefore traces the path where the two states may potentially cross. We also added additional points on either side of each path through a linear extrapolation. In total, each path contains twenty-one geometries obtained through interpolation and extrapolation, as shown in **Fig. 2**.

Single-point calculations along the PESs were performed using TD-DFT with the B3LYP,[100, 101] camB3LYP,[102] and ωB97X-D[103] functionals and the cc-pVTZ basis set. EOM-EE-CCSD and SOS-CIS(D) energies were computed with the cc-pVDZ basis set. MR-PT2 calculations along the scans were also carried out using the ANO-L-VDZP basis set. A [14,12] active space was used for the PESs, comprising two non-bonding orbitals with electron density on the nitrogen atom and five π and five π* orbitals. 3-root state averaging was used for each symmetry and spin.

MP2 and DFT calculations were run using Gaussian16.[104] Multi-configurational calculations were performed with OpenMolcas version 22.10.[105] The density matrix renormalization group (DMRG) calculations for orbital entanglement were run using with the QCMaquis interface with OpenMolcas.[106] The resultant orbital entanglement data were analyzed using autoCAS.[94] EOM-EE-CCSD and SOS-CIS(D) calculations were run using Q-Chem 5.4.[107]

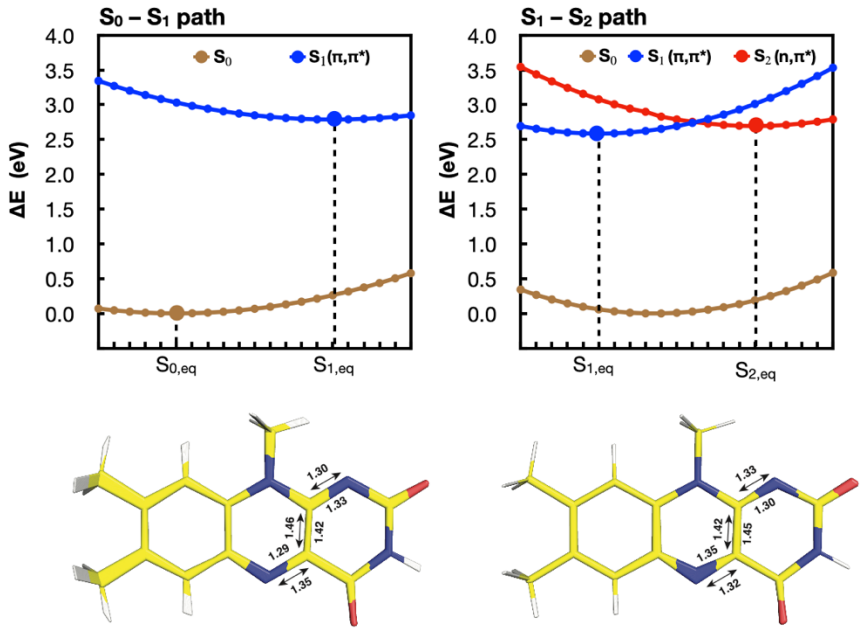

Figure 2: (TD)-B3LYP S_0 (brown), S_1 (blue), and S_2 (red) energies along two paths used for benchmarking electronic structure methods. The S_1 and S_2 labels are conserved throughout the PESs, despite state crossings, to reflect their energy ordering at the ground state equilibrium geometry. The larger circles indicate the minima optimized at the (TD)-B3LYP level of theory. Smaller circles are obtained by linear interpolation and extrapolation. At the bottom of each plot, a figure is shown overlaying the structures of all interpolated and extrapolated geometries. Bond thickness in this figure therefore correlates to the extent of change in coordinates. The labels above and below the structure indicate the bond lengths at the S_0 and S_1 (left) and S_1 and S_2 (right) structures, respectively.

Results and Discussion

The geometries for Fl, $FlH^{\bullet}$, $Fl^{\bullet-}$, FlH^{-}, FlH_2 optimized at the MP2/cc-pVTZ level of theory are compared to the geometries optimized at the B3LYP/cc-pVTZ level of theory from Ref. 21. In **Fig. 3**, we align the molecule along the x-y plane as closely as possible and find the maximum and minimum displacements of heavy atoms along the z-axis. This distance, labeled *d*, indicates the extent of the "butterfly" bending of the isoalloxazine rings in the MP2 and B3LYP geometries for the different redox states. The MP2 and B3LYP geometries are also shown superimposed in the same figure. Even though all molecules were optimized without symmetry constraints, Fl, $FlH^{\bullet}$, and $Fl^{\bullet-}$ remain planar, with only minimal deviations from

planarity. The MP2 and B3LYP geometries are similar, which is also reflected in the TD-B3LYP S_1 excitation energies that differ by no more than 0.05 eV for the two geometries. However, FlH^- and FlH_2 show significantly more bending with MP2 compared to B3LYP. The distance *d* is 1.60 Å for FlH^- at the MP2 level of theory compared to 1.25 Å with B3LYP, while in FlH_2, *d* is 1.32 Å with MP2 compared to 0.76 Å with B3LYP. This manifests in a larger difference in the excitation energies computed with the MP2 and B3LYP geometries (a 0.22 eV difference). Therefore, accurate calculations of thermodynamic quantities or excitation energies for those two reduced states of flavin may necessitate the use of geometries optimized with MP2 or a better level of theory.

Geom	Property	Fl	FlH·	Fl·−	FlH−	FlH_2
B3LYP	*d* (Å)	0.00035	0.00003	0.00008	1.24787	0.76480
B3LYP	$\Delta E_{S_0-S_1}$ (eV)	3.03	2.12	2.11	2.82	3.04
MP2	*d* (Å)	0.00051	0.00124	0.00107	1.59772	1.31796
MP2	$\Delta E_{S_0-S_1}$ (eV)	2.98	2.12	2.10	3.02	3.24

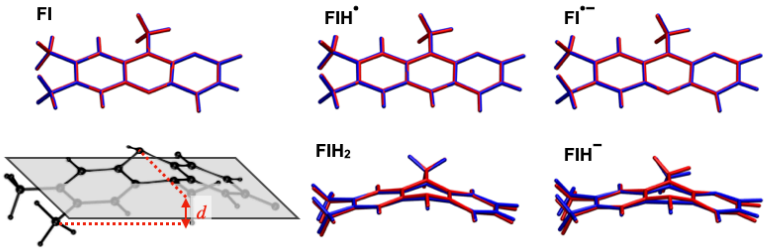

Figure 3: Comparison of geometries and TD-B3LYP/cc-pVTZ excitation energies of flavin in five different redox states optimized with B3LYP and MP2. The schematic at the bottom left panel indicates the definition of the parameter *d*, which is difference in the maximum and minimum positions of heavy atoms along the z axis when the molecules are aligned as closely as possible along the x-y plane. The other five panels show the overlay of the structure for each redox state optimized at the B3LYP (blue) and MP2 (red) levels of theory.

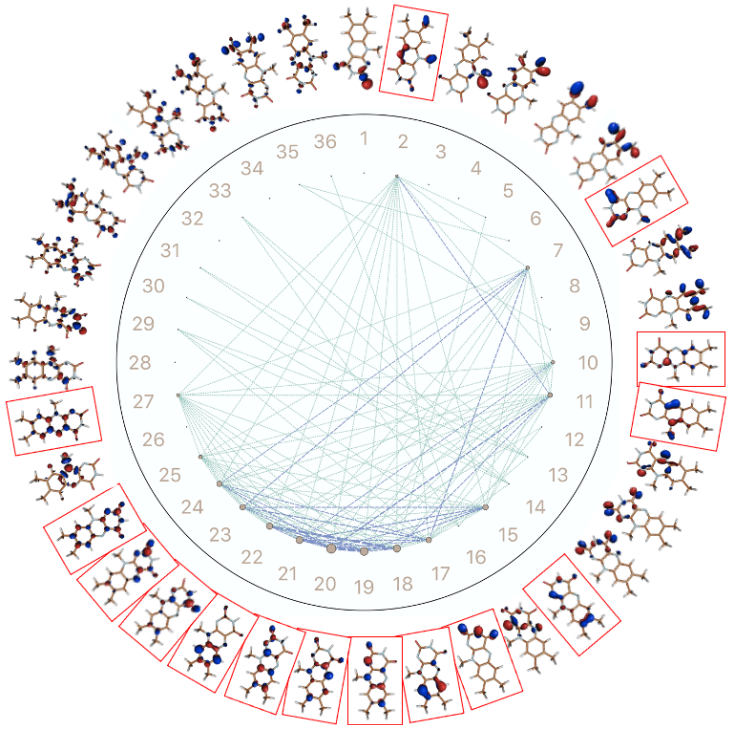

Figure 4: CASSCF-DMRG [38,36] orbital entanglement diagram for oxidized LF. Grey circle size represents the degree of orbital entropy while line thickness indicates mutual information exchange between orbital pairs. Red boxes highlight orbitals with high entropy.

Fig. 4 presents the orbital entanglement diagram for the oxidized form of flavin, which was generated from CASSCF-DMRG wave functions with a [38,36] active space. The diagrams feature a circular arrangement of active orbitals where strong orbital "entropy," a term used in this context to signify a high degree of correlation with other orbitals, is indicated by larger grey circles and mutual information is indicated by the line thickness between the orbitals. A set of 15 orbitals, highlighted in the red boxes in the diagram, exhibited higher single-orbital entropies and mutual information. These orbitals comprise eight bonding π orbitals (16 electrons) and seven anti-bonding π* orbitals, which are shown in **Fig. S1a** of the Supporting Information (SI) document. Consequently, we employed CASSCF with a 16 electron and 15 orbital active space as the starting point for further benchmarking.

While the DMRG-CASSCF calculations indicative the relevance of these 15 orbitals to the molecule's multi-configurational electronic structure, such a large active space makes routine calculations on flavins intractable. This is especially true if one is interested in looking at other excited states such as n,π*, which would necessitate the addition of n orbitals on top of π and π*. Therefore, we examined the effect on the lowest excitation energy of flavin as a function of reducing the active space.

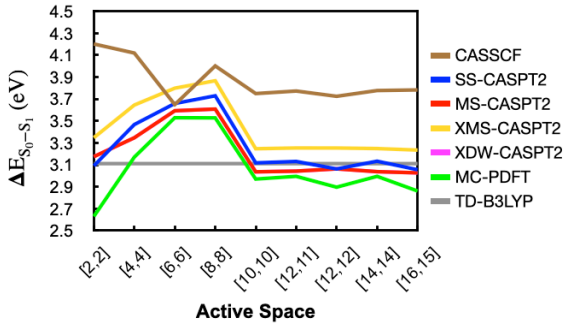

Figure 5: 3-root MR-PT2 and 3-root state averaged CASSCF S_1 excitation energies as a function of active space [number of electrons, number of orbitals] for LF in the oxidized form. A 0.25 IPEA shift is used for MR-PT2 methods. The TD-B3LYP excitation energy is shown as a grey line for reference. XDW-CASPT2 energies are identical to MS-CASPT2 energies in this figure.

In **Fig. 5**, MR-PT2 and MC-PDFT excitation energies are plotted as a function of active space. 3-root state averaging is used for the underlying CASSCF wave function in all cases. The effect of using additional roots is explored further in SI **Fig. S2**, where it is shown that the MR-PT2 energies are relatively stable with the use of three or more states in the CASSCF state averaging. We started with a 16 electron and 15 orbital [16,15] active space shown in **Fig. S1a**. Removing orbitals based on their occupancy had a relatively small impact on S_0-S_1 excitation energies down to a [10,10] active space. However, removing additional orbitals resulted in significant energy variations, indicating unbalanced electron correlation in smaller spaces. A minimal active space of [2,2] gives reasonable excitation energies for most MR-PT2 methods,

as has been also shown by Domratcheva and co-workers.[53, 57] Overall, the results in **Fig. 5** suggest that a [10,10] active space is sufficient for accurate π,π* excitation energy calculations when using the orbitals labeled as π_1, π_2, π_3, π_4, π_5, π_1*, π_2*, π_3*, π_4*, and π_5* in **Fig. S1a**. SS-CASPT2, MS-CASPT2, and XDW-CASPT2 provide largely consistent energies. XMS-CASPT2 gives energies that are consistently 0.2 eV above those methods, while MC-PDFT gives energies that are around 0.1 to 0.25 eV below these methods, depending on the active space used.

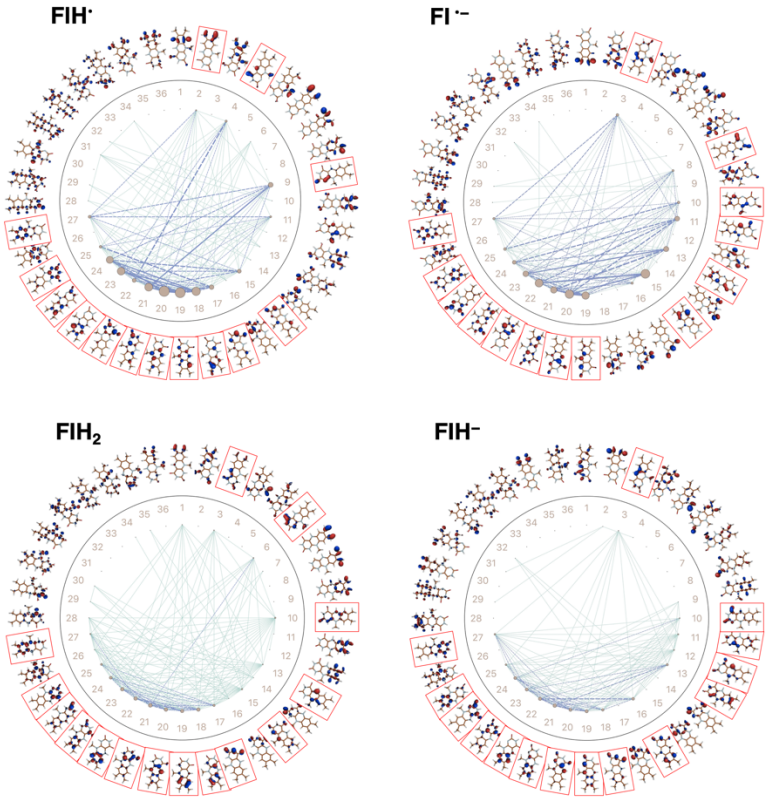

Figure 6: Orbital entanglement diagram for the semiquinone and hydroquinone reduced forms of LF. CASSCF-DMRG [39,36] actives spaces were used for the semiquinones and [40,36] for the hydroquinones. Grey circle size represents the degree of orbital entropy while line thickness indicates mutual information exchange between orbital pairs. Red boxes highlight orbitals with high entropy.

In **Fig. 6**, we show AutoCAS maps constructed from CASSCF-DMRG wave function calculations on $FlH^{\bullet}$, $Fl^{\bullet-}$, FlH_2, and FlH^{-}. The calculations for $FlH^{\bullet}$ and $Fl^{\bullet-}$ use a [39,36] active space, while those for FlH_2 and FlH^{-} use a [40,36] active space. We find that eight bonding and six anti-bonding orbitals are important for both $FlH^{\bullet}$ and $Fl^{\bullet-}$. For FlH_2 and FlH^{-}, nine bonding and six anti-bonding orbitals with high entropy were found instead. These orbitals are highlighted in red boxes and are shown in SI **Figs. S1b-S1e** along with their occupancies.

We computed the excitation energies for these four redox and protonation states as a function of decreasing active space size by sequentially removing the highest occupancy orbitals, as we did for Fl. The excitation energies obtained from these calculations, along with TD-B3LYP energies, are shown in **Fig. 7**.

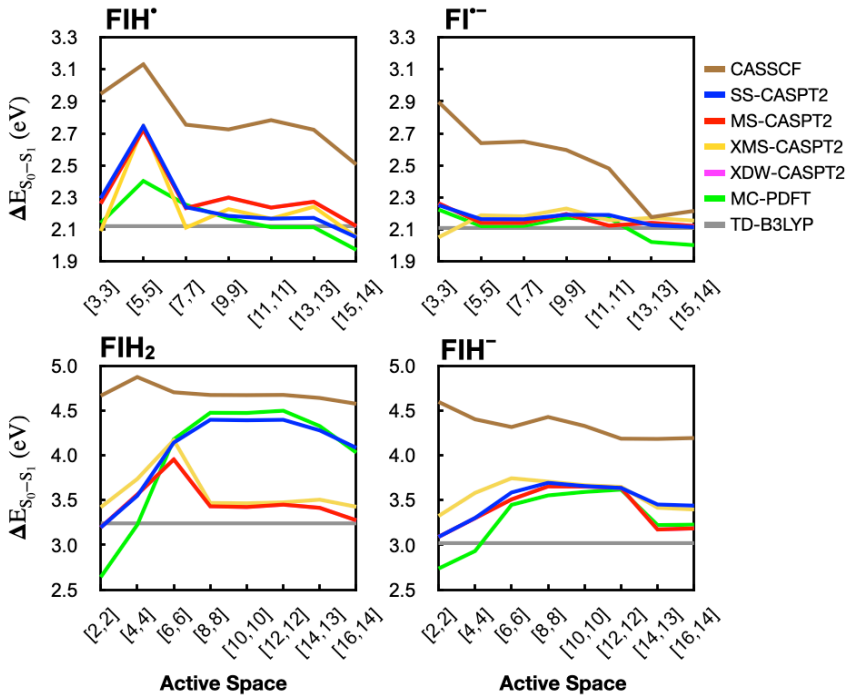

Figure 7: 3-root MR-PT2 and 3-root state averaged CASSCF S_1 excitation energies as a function of active space [number of electrons, number of orbitals] for LF in different redox states. The IPEA=0.25 shift is used for all MR-PT2 methods. The redox state is indicated above each panel. The TD-B3LYP excitation energy is shown as a grey line for reference. XDW-CASPT2 energies are identical to MS-CASPT2 energies in these figures.

For $FlH^{\bullet}$ and $Fl^{\bullet-}$, the MR-PT2 and MC-PDFT calculations with large active spaces gave results largely similar to TD-B3LYP. For $FlH^{\bullet}$, reducing the active space size had a limited effect down to a [7,7] active space. A minimal active space, [3,3], also gives similar results, but a [5,5] active space appears imbalanced. In FlH^{-}, on the other hand, any active space [3,3] or larger gave similar energies.

In FlH_2, and FlH^{-}, which have non-planar geometries, the convergence of the excitation energies with increasing active space size is much less smooth compared to the other states. Up to the largest active space tested, [16,14], there continue to be changes in the excitation energies. This may be attributed to the bent structure of these two redox states, which allow mixing between non-bonded or sigma orbitals with π orbitals that likely results in stronger correlation between a larger set of orbitals. This can be seen to some extent in the autoCAS maps in **Fig. 6**, where FlH_2 and FlH^{-} have more orbitals involved in the mutual information exchange, even though the degree of entanglement is smaller for each orbital.

In FlH_2, there is a large difference of ca. 1.0 eV between the MC-PDFT and SS-CASPT2 results compared to those calculated with MS/XMS/XDW-CASPT2. Such differences between SS-CASPT2 and MS-CASPT2 have been previously discussed[45] and are usually resolved through the XMS or XDW extension to these theories, as appears to be the case here.

PESs for Flavin's Low-Lying Excited States

For the application of electronic structure methods towards studying the photophysics of flavin, it is important to move beyond single point energy calculations and to explore the energies of different methods along relevant coordinates. Here, we focus on PESs near flavin's Franck-Condon region along two modes (**Fig. 2**). One mode (S_0–S_1) connects the geometries of the S_0

and S_1 minima optimized at the (TD)-B3LYP/cc-pVTZ level of theory. The second mode (S_1 – S_2) connects the S_1 and S_2 minima optimized at the TD-B3LYP/cc-pVTZ level of theory. The aim is to check the sensitivity of the relative energies, curvatures, and crossing points of the low-lying singlet and triplet excited states along these paths to the electronic structure method.

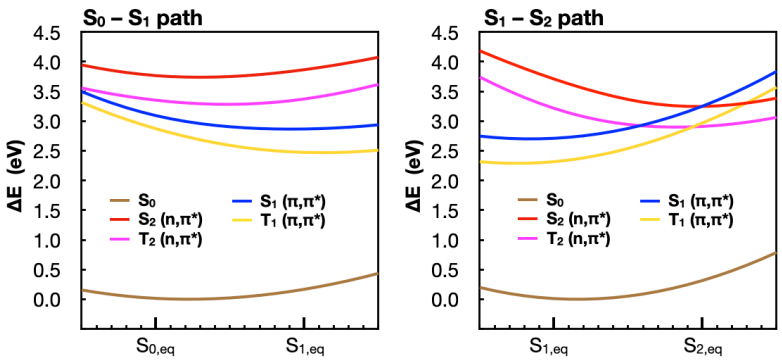

Figure 8: 3-root MS-CAPT2(IPPEA=0.25)[14,12]/ANO-L-VDZP S_0 (brown), S_1 (blue), S_2 (red), T_1 (yellow) and T_2 (magenta) energies along the S_0–S_1 path (left) and the S_1–S_2 path (right).

In **Fig. 8**, we show MS-CASPT2 energies for five states (S_0, S_1, S_2, T_1, and T_2) along the two paths. The [14,12] active space comprises the 5 π and 5 π* orbitals consistent with the [10,10] active space from **Fig. 5** plus two non-bonding orbitals localized on the N_1 and N_5 nitrogen atoms. S_1 is the optically active π,π* state, while S_2 is the optically inactive n,π* state involving the non-bonding orbitals. The triplet states, T_1 and T_2, have the same electronic transitions as the S_1 and S_2 states, respectively. The S_1 state crosses with both the S_2 and the T_2 states along the S_1–S_2 path,.

We first focus on the S_0 and S_1 PESs along the S_0–S_1 path, since those two states are responsible for the spectroscopic properties of flavin's first excitation band. We then shift our focus to the S_1, S_2, and T_2 PESs along the S_1–S_2 path, since their crossings represent possible internal conversion (IC) or ISC points, respectively.

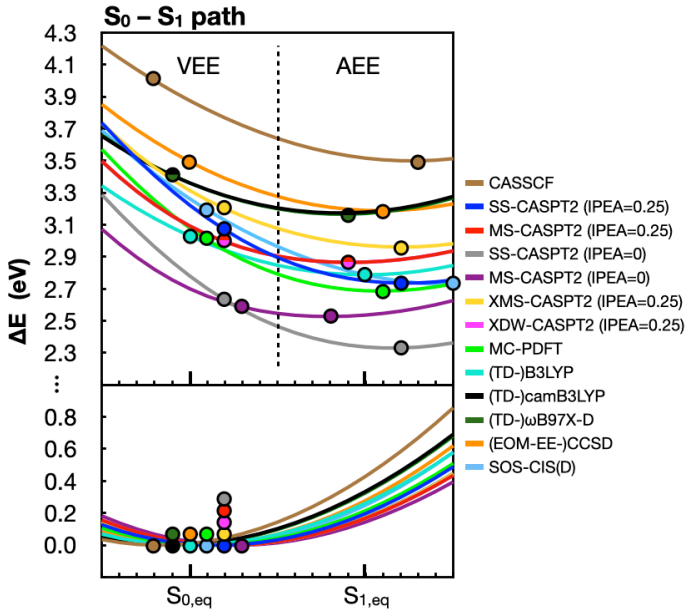

Figure 9: S_0 (bottom) and S_1 (top) energies along the S_0–S_1 path reported relative to the corresponding S_0 minimum energy point along the path. Energies are shown for 3-root state averaged CASSCF, MR-PT2, MC-PDFT, TD-DFT, EOM-EE-CCSD, and SOS-CIS(D) methods, using colors indicated in the legend on the right. CASSCF and MR-PT2 energies employ a [14,12] active space. In the bottom panel, the circles indicate the interpolated geometry that has the lowest energy for each method. In the top panel, circles indicate the corresponding vertical excitation energy (VEE, left side) and the adiabatic excitation energy (AEE, right side) along this path. The latter is found as the point with the lowest S_1 energy along the path. XDW-CASPT2 energies are identical to MS-CASPT2 energies in this figure.

Fig. 9 plots the S_0 and S_1 energies along the S_0–S_1 path with different methods. For S_0, CASSCF stands out from other curves at large distortion. This is likely due to missing dynamical electron correlation, particularly sigma orbitals that become involved with bond stretching. However, even among other methods that do account for dynamical electron correlation, we find that there are differences in the positions of the S_0 minima along the PES. CCSD is the only other method that has the same minimum point as the B3LYP-optimized S_0 state. Conversely, camB3LYP and ωB97X-D give geometries that are further away from the S_1 minimum and fall along the extrapolated portion of the PES. MR-PT2, MC-PDFT, and SOS-CIS(D) methods, on the other hand give minima that are closer to the S_1 equilibrium structure. Non-parallelity errors

(NPEs), which are reported relative to the XDW-CASPT2 (IPEA=0.25) energy profile, reflect those differences as well (**Table 1**). NPEs are calculated as the largest deviation from the reference XDW-CASPT2 curve minus the smallest deviation from the same curve. Methods that have similar minimum points to XDW-CASPT2 and have similar curvature have small S_0 NPEs, while methods with different minimum energy geometries display larger S_0 NPEs.

	S_0 NPE (eV)	**S_1 NPE (eV)**
CASSCF	0.54	0.21
SS-CASPT2 (IPEA=0.25)	0.08	0.42
MS-CASPT2 (IPEA=0.25)	0.00	0.00
SS-CASPT2 (IPEA=0)	0.03	0.37
MS-CASPT2 (IPEA=0)	0.07	0.11
XMS-CASPT2	0.02	0.19
MC-PDFT	0.12	0.28
(TD-)B3LYP	0.23	0.10
(TD-)camB3LYP	0.37	0.18
(TD-) ω B97X-D	0.35	0.17
EOM-EE-CCSD	0.26	0.11
SOS-CIS(D)	0.20	0.41

Table 1: NPEs for different methods calculated relative to the reference XDW-CASPT2 PES.

The differences between methods become substantially more pronounced when looking at the S_1 state, both in terms of the excitation energy as well as the shape (curvature) of the excited state potential energy surface along this path. Vertical excitation energies (VEEs), which are indicated with circles in the top left section of **Fig. 9**, reflect the S_0-S_1 energy differences at the same position where a method's S_0 minimum is found. Even if we exclude CASSCF from the analysis due to its missing dynamical electron correlation, we find that VEEs vary from 2.59 eV (MS-CASPT2 with IPEA=0) to 3.49 eV (EOM-EE-CCSD), a range of 0.90 eV. Changes in the curvature of the excited state potential energy surface are reflected by the S_1 NPEs shown in **Table 1**. While some excited state methods have PESs that resemble the XDW-CASPT2 PES (S_1 NPE within 0.11 eV), several methods stand out has having a different curvature along this

path. Specifically, SS-CASPT2 (NPE=0.37-0.42 eV), SOS-CIS(D) (NPE=0.41 eV), MC-PDFT (NPE=0.28 eV), and XMS-CASPT2 (NPE=0.19 eV) all have a larger curvature compared to XDW-CASPT2. On the other hand. TD-DFT methods, which give NPEs ranging from 0.10 to 0.18, have smaller curvature.

In the top right part of **Fig. 9**, circles are used to indicate the S_1 minima for the different methods calculated along the S_0–S_1 path. The ΔE value at those points reflects the adiabatic excitation energies (AEEs) for the different methods. We note that those are approximate AEEs because they are not true minima but instead are the lowest energy points computed along a TD-B3LYP PES. Nonetheless, there is a marked variation in these energies, which is a result of both the differences in the VEEs as well as the differences in curvatures of the different methods. AEEs along this path range from 2.33 eV (CASPT2 with IPEA=0) to 3.19 eV for EOM-EE-CCSD, a 0.86 eV range.

In **Fig. 10**, we plot S_0, S_1, S_2, and T_2 energies along the S_1–S_2 path. The circles on the S_0 PES again indicate differences in the positions of the minima for the different methods, which all lie somewhere between the S_1 and S_2 geometries. In the top left panel of **Fig. 10**, we show both the S_1 and S_2 states. For all methods shown, the two states cross at some point along the S_1–S_2 path. In all cases, the S_1 minimum remains lower in energy than the S_2 minimum, suggesting (at least, in the gas phase) that the S_2 (n,π*) state would not get populated from the S_1 state. Since solvents typically stabilize (red-shift) π,π* excited states and destabilize (blue-shift) n,π* states,[108] we expect the same conclusion will also apply to flavins in solution. The S_1/S_2 crossings for all methods, indicated using circles, are geometrically closer to the S_2 minima and often lie well above the S_1 minima. In **Table 2** we tabulate $\Delta E_{S_1/S_2}$, which are energy differences between the S_1/S_2 crossing points and the S_1 minima, for the different methods.

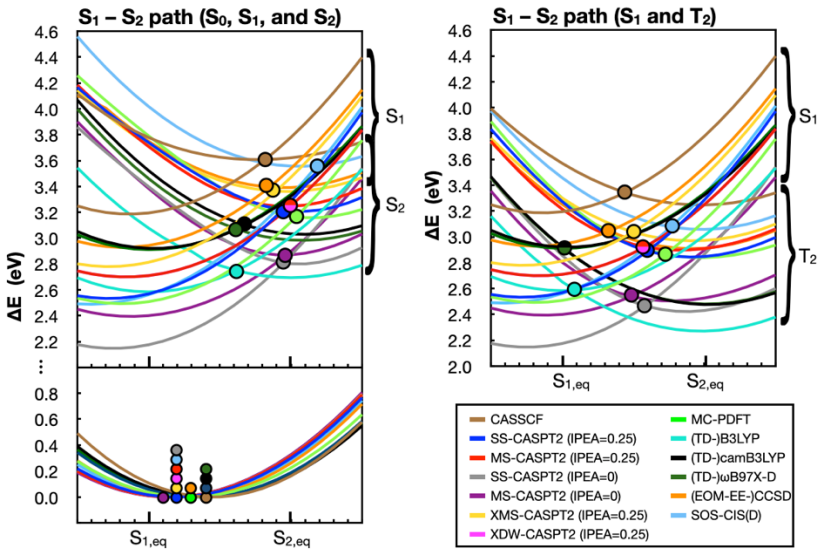

Figure 10: PESs along the S_1–S_2 path. In the left panel, we show the S_0 (bottom left panel) as well as S_1 and S_2 (top left panel) potential energies reported relative to the corresponding S_0 minimum energy point along this path. In the panel on the right, we show the S_1 and T_2 energies along the same path. Energies are shown for 3-root state averaged CASSCF, MR-PT2, MC-PDFT, TD-DFT, EOM-EE-CCSD, and SOS-CIS(D) methods, using colors indicated in the legend on the bottom right. MR-PT2 and CASSCF energies employ a [14,12] active space. In the bottom left panel, the circles indicate the interpolated geometry that has the lowest energy. In the tops panels, circles indicate crossing points between the S_1 state and the S_2 (left) or T_2 (right) states. XDW-CASPT2 energies are identical to MS-CASPT2 energies in these figures.

The S_1/T_2 plots (**Fig. 10** right) tell a different story. There, the relative energies of the S_1 and T_2 minima are more comparable, with some methods showing a lower S_1 state minimum energy point and other methods showing a lower T_2 minimum. For example, TD-DFT methods show that the T_2 minimum is lower than the S_1 minimum, while MR-PT2 methods show that the S_1 minimum is lower than T_2. The S_1/T_2 crossings lie somewhere in the middle between the two coordinates. As discussed by Salzmann et al. in multiple studies,[36, 76, 77] solvent effects or a protein environment can play an important role in changing flavin's photophysics by modulating the relative energies of the S_1 and T_2 states. However, here we also find that the relative energies of those states are sensitive to the choice of computational method.

Table 2 presents $\Delta E_{S_1/T_2}$, the relative energies of the S_1/T_2 ISC point compared to the S_1 minimum along the S_1–S_2 path, alongside the corresponding $\Delta E_{S_1/S_2}$ values. These may not be the lowest energy crossing point for each method, but the variations in these numbers for the different methods indicates either that 1) the barrier to those crossings is different for the different methods, or 2) the minimum energy crossing geometry varies from one method to another. For example, along the S_1–S_2 path, TD-DFT methods indicate that the S_1/T_2 ISC point coincides with the S_1 minimum geometry (with a barrier of ~0 eV) while SOS-CIS(D) gives a $\Delta E_{S_1/T_2}$ of 0.62 eV. EOM-EE-CCSD gives a $\Delta E_{S_1/T_2}$ of 0.10 eV while MR-PT2 methods give $\Delta E_{S_1/T_2}$ values that vary from 0.23 to 0.36 eV.

When looking more generally at the trends in both $\Delta E_{S_1/S_2}$ and $\Delta E_{S_1/T_2}$, most MR-PT2 methods and MC-PDFT appear to treat the singlet and triplet π,π* and n,π* states on a similar footing, since the crossing geometries do not change considerably from one method to the other. The IPEA shift has a large effect on the S_1, S_2, and T_2 energies relative to the reference S_0 state, but it does not have much of an impact on their energies relative to each other since all three states have similarly open-shell character. This is results in $\Delta E_{S_1/S_2}$ and $\Delta E_{S_1/T_2}$ barriers for the IPEA=0 calculations that are comparable in magnitude to their IPEA=0.25 counterparts. TD-DFT methods, on the other hand, predict lower energies for both the S_2 and T_2 (n,π*) states, give crossing geometries that are closer to the S_1 minimum, and have considerably smaller $\Delta E_{S_1/S_2}$ and $\Delta E_{S_1/T_2}$ energies. EOM-EE-CCSD gives crossing geometries and $\Delta E_{S_1/S_2}$ and $\Delta E_{S_1/T_2}$ energies that are intermediate between those of TD-DFT and MR-PT2. SOS-CIS(D), on the other hand, appears to significantly overestimate $\Delta E_{S_1/S_2}$ and $\Delta E_{S_1/T_2}$ compared to the other methods. We note that EOM-EE-CCSD and SOS-CIS(D) calculations were carried out with a smaller basis set (double-ζ instead of triple-ζ), which may contribute to the difference observed.

Method	$\Delta E_{S_1/S_2}$(eV)	$\Delta E_{S_1/T_2}$(eV)
CASSCF	0.40	0.13
SS-CASPT2 (IPEA=0.25)	0.64	0.36
MS-CASPT2 (IPEA=0.25)	0.55	0.23
SS-CASPT2 (IPEA=0)	0.66	0.33
MS-CASPT2 (IPEA=0)	0.50	0.15
XMS-CASPT2 (IPEA=0.25)	0.59	0.26
XDW-CASPT2 (IPEA=0.25)	0.55	0.23
MC-PDFT	0.63	0.35
TD-B3LYP	0.15	0.00
TD-camB3LYP	0.19	0.00
TD-ωB97X-D	0.15	0.00
EOM-EE-CCSD	0.47	0.10
SOS-CIS(D)	1.09	0.62

Table 2: Energy barrier to the S_1/S_2 crossing point ($\Delta E_{S_1/S_2}$) and the S_1/T_2 crossing point ($\Delta E_{S_1/T_2}$) relative to the S_1 minimum energy. Those barriers are estimated for different electronic structure methods along the S_1–S_2 path.

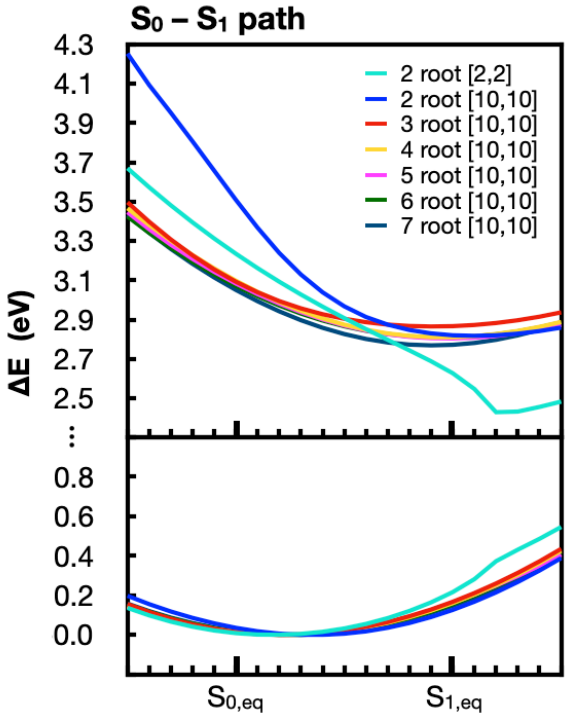

Figure 11: S_0 (bottom panel) and S_1 (top panel) energies along the S_0–S_1 path reported relative to the corresponding S_0 minimum energy point along the path. Energies are shown for MS-CASPT2 with IPEA=0.25 but with different number of roots used in the state averaging of the underlying CASSCF wave function. We also include one calculation where the minimal [2,2] active space is used instead of [10,10].

In **Fig. 11**, we show the energy profiles computed using MS-CASPT2 (IPEA=0.25) with different state averaging or active space along the S_0–S_1 path. Using 3 or more states in the zeroth-order CASSCF wave function gives comparable S_0 and S_1 energy profiles along this path. However, using 2-root state averaging gives a qualitatively different S_1 energy profile. Similarly, using a minimal [2,2] active space, while successful at reproducing the vertical excitation energy of flavin, has a distorted S_0 and S_1 PES when moving away from the S_0 equilibrium structure. This may result in artefacts far from the Franck-Condon region.

Conclusion

Multiple computational studies have investigated the excited-state electronic structure and photophysics of flavin. A non-exhaustive list includes Refs. 21, 36-39, 50-81. A more comprehensive list of computational studies can be found in a recent review article by Kar, Miller, and Mroginski.[78] These studies employ a range of computational methods including semi-empirical, TD-DFT, coupled cluster, and multi-configurational approaches. Even among multi-configurational studies, methodological details such as the number of roots used in state averaging or the size of the active space may differ. With the continued advancement in the use of flavins and flavoproteins for novel photocatalytic, sensing, and biotechnological applications,[31, 109-115] we expect that computational studies on these systems will continue to elucidate and guide experimental studies. In this work, we present a comparison of how different electronic structure methods describe the energetics of the low-lying excited states of flavin.

In the first part of this study, we compared S_1 excitation energies calculated with MR-PT2 methods and those computed with TD-B3LYP for flavin in different redox and protonation states. We focus on the S_1 state because, according to Kasha's rule, this is the state from which a system's photophysics and photochemistry typically occurs. An initial active space for

CASSCF and MR-PT2 calculations is selected using autoCAS, but then the number of orbitals in the active space are gradually reduced to check the effect on the S_0-S_1 excitation energy. Here, TD-B3LYP serves as a reasonable reference since it has been well tested against experimental spectra and shown to agree well when properly accounting for Franck-Condon factors.[21, 38, 39, 61, 67] For most redox states, MS-CASPT2 (with the IPEA 0.25 shift) agrees well with TD-B3LYP excitation energies if a sufficiently large basis set is used. For the oxidized and semi-quinone forms of flavin, which are planar, the convergence of the excitation energy is reached quickly with a small or moderate active space size. In the case of the hydroquinone forms of flavin, which are bent, a larger active space is needed for MR-PT2 methods to converge. For SS-CASPT2 and MC-PDFT, convergence with increasing active space size is not achieved for FlH_2 even when using a 16 electron and 14 orbital active space.

In the second part of this work, we compare TD-DFT, EOM-EE-CCSD, SOS-CIS(D), MC-PDFT, and MR-PT2 energy profiles along a PES connecting the S_0 and S_1 equilibrium geometries (i.e., tracing the Franck-Condon active mode) and along a PES connecting the S_1 (π,π^*) and S_2 (n,π^*) minima. Along the S_0–S_1 path, we find that (TD)-B3LYP is in reasonably good agreement with MS-CASPT2 (IPEA=0.25) energies, which explains its success in simulating UV-visible spectra. However, the same is not true for the S_1–S_2 path, where (TD)-B3LYP has a significantly lower energy for the S_2 and T_2 states compared to MS-CASPT2 (IPEA=0.25). camB3LYP and ωB97X-D, which are hybrid functionals that include a long-range correction that is missing in B3LYP, appear to have a reduced agreement with multi-reference methods.

While MS-CASPT2 with a minimal [2,2] active space and/or 2-root state averaging can give VEEs that are in good agreement with larger active spaces, it is not recommended for studying regions far from the Franck-Condon point.

For all methods tested, the S_2 minimum lies above the S_1 minimum, suggesting that it is unlikely to be involved in flavin's photophysics. The T_2 (n,π*) state, on the other hand, may be populated by ISC from the S_1 (π,π*) state. There relative energies of those states are sensitive to the choice of computational method, and we posit that additional benchmarking is needed for a more quantitative description of ISC in flavins.

Earlier work with Olivucci and co-workers resulted in a series of benchmark studies on a minimal three double-bond reduced model of the retinal protonated Schiff base chromophore of rhodopsins (PSB3).[116-123] Some of this work is reviewed in Ref. 124. There, energies and wavefunctions of a wide range of methods were compared along paths relevant to PSB3's isomerization coordinate and S_1 excited-state dynamics. Here, we again emphasize the usefulness of moving beyond vertical energies or energy differences between two points in benchmark studies. Instead, by comparing methods along a reaction or photophysical pathway, important differences in how these methods treat different regions of a potential energy surface may emerge. For PSB3, methods that could accurately reproduce the VEE could not necessarily describe the twisted PSB3 intermediates, which either displayed strong charge transfer character or diradical character. On the other hand, a few methods could treat both the planar and fully twisted PSB3 intermediates well but deteriorated when describing intermediate structures connecting the planar and 90° twisted geometries. Ultimately, through extensive benchmarks, methods were found that have a suitable error cancellation to treat different regions of PSB3's

potential energy surface on a similar footing. This has enabled, for instance, the construction of model potentials suitable for running quantum dynamics for PSB3.[125] Similarly, additional benchmark studies on flavin can lead to the adoption of methods that may be used routinely for studying the photophysics and photochemistry of this system in different protein environments.

Data Availability

The main data from this work are presented in the manuscript and in the supporting information. Requests for additional data, including computational models and raw data files, should be directed to S.G. (sgozem@gsu.edu).

Supporting Information

Figures of the molecular orbitals included in the active space of CASSCF and MR-PT2 calculations; Plots of CASSCF S_1 excitation energies as a function of active space and number of roots used in the state averaging for LF in the oxidized form (PDF)

Acknowledgements

This material is based upon work supported by the National Science Foundation (NSF) under Grant CHE-2047667 (S.G.). M.P.K. acknowledge a fellowship from the Molecular Basis of Disease Program at Georgia State University. M.P.K. also acknowledges support from the Provost Dissertation Fellowship at Georgia State University. This work used Expanse at SDSC through allocation CHE180027 from the Advanced Cyberinfrastructure Coordination Ecosystem: Services and Support (ACCESS) program, which is supported by National Science Foundation grants 2138259, 2138286, 2138307, 2137603, and 2138296. We also acknowledge

the use of Advanced Research Computing Technology and Innovation Core (ARCTIC) resources at Georgia State University's Research Solutions, made available by the NSF Major Research Instrumentation (MRI) grant number CNS-1920024.

Author Contributions

M.P.K.: Data curation, formal analysis, investigation, validation, visualization, writing – original draft. P.G.: Data curation, formal analysis, investigation, validation, visualization, writing – review & editing. S.G.: Conceptualization, funding acquisition, project administration, resources, supervision, validation, visualization, writing – review & editing.

Conflict of Interest

The authors declare that they have no conflicts of interest with the contents of this article.

References

1. Albert, A., Quantitative studies of the avidity of naturally occurring substances for trace metals. 3. Pteridines, riboflavin and purines. *Biochemical Journal* **1953,** *54* (4), 646.
2. Draper, R. D.; Ingraham, L. L., A potentiometric study of the flavin semiquinone equilibrium. *Archives of Biochemistry and Biophysics* **1968,** *125* (3), 802-808.
3. Zheng, Y.; Carey, P. R.; Palfey, B. A., Raman spectrum of fully reduced flavin. *Journal of Raman Spectroscopy* **2004,** *35* (7), 521-524.
4. Mansoorabadi, S. O.; Thibodeaux, C. J.; Liu, H. W., The diverse roles of flavin coenzymes--nature's most versatile thespians. *J Org Chem* **2007,** *72* (17), 6329-42.
5. Romero, E.; Gomez Castellanos, J. R.; Gadda, G.; Fraaije, M. W.; Mattevi, A., Same Substrate, Many Reactions: Oxygen Activation in Flavoenzymes. *Chem Rev* **2018,** *118* (4), 1742-1769.
6. Massey, V., The chemical and biological versatility of riboflavin. *Biochemical Society Transactions* **2000,** *28* (4), 283-296.
7. Walsh, C. T.; Wencewicz, T. A., Flavoenzymes: versatile catalysts in biosynthetic pathways. *Nat Prod Rep* **2013,** *30* (1), 175-200.
8. Tomiki, T.; Saitou, N., Phylogenetic analysis of proteins associated in the four major energy metabolism systems: photosynthesis, aerobic respiration, denitrification, and sulfur respiration. *J Mol Evol* **2004,** *59* (2), 158-76.
9. Forti, G., Flavoproteins. In *Photosynthesis I*, Springer: 1977; pp 222-226.
10. Helman, Y.; Tchernov, D.; Reinhold, L.; Shibata, M.; Ogawa, T.; Schwarz, R.; Ohad, I.; Kaplan, A., Genes encoding A-type flavoproteins are essential for photoreduction of O2 in cyanobacteria. *Current Biology* **2003,** *13* (3), 230-235.
11. James, W. O., The terminal oxidases of plant respiration. *Biological Reviews* **1953,** *28* (2), 245-260.

12. Herrmann, G.; Jayamani, E.; Mai, G.; Buckel, W., Energy conservation via electron-transferring flavoprotein in anaerobic bacteria. *Journal of bacteriology* **2008,** *190* (3), 784-791.
13. van Spanning, R. J.; Richardson, D. J.; Ferguson, S. J., Introduction to the biochemistry and molecular biology of denitrification. In *Biology of the nitrogen cycle*, Elsevier: 2007; pp 3-20.
14. Delwiche, C.; Bryan, B. A., Denitrification. *Annual Review of Microbiology* **1976,** *30* (1), 241-262.
15. Ahmad, M.; Cashmore, A. R., HY4 gene of A. thaliana encodes a protein with characteristics of a blue-light photoreceptor. *Nature* **1993,** *366* (6451), 162-166.
16. Christie, J. M.; Salomon, M.; Nozue, K.; Wada, M.; Briggs, W. R., LOV (light, oxygen, or voltage) domains of the blue-light photoreceptor phototropin (nph1): binding sites for the chromophore flavin mononucleotide. *Proceedings of the National Academy of Sciences* **1999,** *96* (15), 8779-8783.
17. Gomelsky, M.; Klug, G., BLUF: a novel FAD-binding domain involved in sensory transduction in microorganisms. *Trends in biochemical sciences* **2002,** *27* (10), 497-500.
18. Sancar, A., Structure and function of DNA photolyase. *Biochemistry* **1994,** *33* (1), 2-9.
19. Seth, D., Photoenzymic repair of UV-damaged DNA: a chemist's perspective. *Chemical Society Reviews* **1995,** *24* (4), 289-297.
20. Schwinn, K.; Ferré, N.; Huix-Rotllant, M., UV-visible absorption spectrum of FAD and its reduced forms embedded in a cryptochrome protein. *Physical Chemistry Chemical Physics* **2020,** *22* (22), 12447-12455.
21. Kabir, M. P.; Orozco-Gonzalez, Y.; Gozem, S., Electronic spectra of flavin in different redox and protonation states: a computational perspective on the effect of the electrostatic environment. *Physical Chemistry Chemical Physics* **2019,** *21* (30), 16526-16537.
22. Kottke, T.; Hegemann, P.; Dick, B.; Heberle, J., The photochemistry of the light-, oxygen-, and voltage-sensitive domains in the algal blue light receptor phot. *Biopolymers: Original Research on Biomolecules* **2006,** *82* (4), 373-378.
23. Swartz, T. E.; Corchnoy, S. B.; Christie, J. M.; Lewis, J. W.; Szundi, I.; Briggs, W. R.; Bogomolni, R. A., The photocycle of a flavin-binding domain of the blue light photoreceptor phototropin. *Journal of Biological Chemistry* **2001,** *276* (39), 36493-36500.
24. Kasha, M., Characterization of electronic transitions in complex molecules. *Discussions of the Faraday society* **1950,** *9*, 14-19.
25. Chapman, S.; Faulkner, C.; Kaiserli, E.; Garcia-Mata, C.; Savenkov, E. I.; Roberts, A. G.; Oparka, K. J.; Christie, J. M., The photoreversible fluorescent protein iLOV outperforms GFP as a reporter of plant virus infection. *Proceedings of the National Academy of Sciences* **2008,** *105* (50), 20038-20043.
26. Christie, J. M.; Hitomi, K.; Arvai, A. S.; Hartfield, K. A.; Mettlen, M.; Pratt, A. J.; Tainer, J. A.; Getzoff, E. D., Structural tuning of the fluorescent protein iLOV for improved photostability. *Journal of Biological Chemistry* **2012,** *287* (26), 22295-22304.
27. Mukherjee, A.; Schroeder, C. M., Flavin-based fluorescent proteins: emerging paradigms in biological imaging. *Current opinion in biotechnology* **2015,** *31*, 16-23.
28. Westberg, M.; Holmegaard, L.; Pimenta, F. M.; Etzerodt, M.; Ogilby, P. R., Rational design of an efficient, genetically encodable, protein-encased singlet oxygen photosensitizer. *Journal of the American Chemical Society* **2015,** *137* (4), 1632-1642.
29. Li, X.; Page, C. G.; Zanetti-Polzi, L.; Kalra, A. P.; Oblinsky, D. G.; Daidone, I.; Hyster, T. K.; Scholes, G. D., Mechanism and dynamics of photodecarboxylation catalyzed by lactate monooxygenase. *Journal of the American Chemical Society* **2023,** *145* (24), 13232-13240.
30. Su, D.; Smitherman, C.; Gadda, G., A Metastable Photoinduced Protein–Flavin Adduct in Choline Oxidase, an Enzyme Not Involved in Light-Dependent Processes. *The Journal of Physical Chemistry B* **2020,** *124* (19), 3936-3943.
31. Zhuang, B.; Liebl, U.; Vos, M. H., Flavoprotein photochemistry: fundamental processes and photocatalytic perspectives. *The Journal of Physical Chemistry B* **2022,** *126* (17), 3199-3207.
32. Campbell, A. C.; Prater, A. R.; Bogner, A. N.; Quinn, T. P.; Gates, K. S.; Becker, D. F.; Tanner, J. J., Photoinduced Covalent Irreversible Inactivation of Proline Dehydrogenase by S-Heterocycles. *ACS Chem Biol* **2021,** *16* (11), 2268-2279.
33. Potzkei, J.; Kunze, M.; Drepper, T.; Gensch, T.; Jaeger, K.-E.; Büchs, J., Real-time determination of intracellular oxygen in bacteria using a genetically encoded FRET-based biosensor. *BMC biology* **2012,** *10* (1), 28.
34. Shu, X.; Lev-Ram, V.; Deerinck, T. J.; Qi, Y.; Ramko, E. B.; Davidson, M. W.; Jin, Y.; Ellisman, M. H.; Tsien, R. Y., A genetically encoded tag for correlated light and electron microscopy of intact cells, tissues, and organisms. *PLoS biology* **2011,** *9* (4).

35. Ruiz-González, R. n.; Cortajarena, A. L.; Mejias, S. H.; Agut, M.; Nonell, S.; Flors, C., Singlet oxygen generation by the genetically encoded tag miniSOG. *Journal of the American Chemical Society* **2013,** *135* (26), 9564-9567.
36. Salzmann, S.; Silva-Junior, M. R.; Thiel, W.; Marian, C. M., Influence of the LOV domain on low-lying excited states of flavin: a combined quantum-mechanics/molecular-mechanics investigation. *The Journal of Physical Chemistry B* **2009,** *113* (47), 15610-15618.
37. Neiss, C.; Saalfrank, P.; Parac, M.; Grimme, S., Quantum chemical calculation of excited states of flavin-related molecules. *The Journal of Physical Chemistry A* **2003,** *107* (1), 140-147.
38. Klaumünzer, B.; Kröner, D.; Saalfrank, P., (TD-) DFT calculation of vibrational and vibronic spectra of riboflavin in solution. *The Journal of Physical Chemistry B* **2010,** *114* (33), 10826-10834.
39. Davari, M. D.; Kopka, B.; Wingen, M.; Bocola, M.; Drepper, T.; Jaeger, K. E.; Schwaneberg, U.; Krauss, U., Photophysics of the LOV-Based Fluorescent Protein Variant iLOV-Q489K Determined by Simulation and Experiment. *J Phys Chem B* **2016,** *120* (13), 3344-52.
40. Roos, B. O.; Taylor, P. R.; Sigbahn, P. E., A complete active space SCF method (CASSCF) using a density matrix formulated super-CI approach. *Chemical Physics* **1980,** *48* (2), 157-173.
41. Andersson, K.; Malmqvist, P. A.; Roos, B. O.; Sadlej, A. J.; Wolinski, K., Second-order perturbation theory with a CASSCF reference function. *Journal of Physical Chemistry* **1990,** *94* (14), 5483-5488.
42. Finley, J.; Malmqvist, P.-Å.; Roos, B. O.; Serrano-Andrés, L., The multi-state CASPT2 method. *Chemical physics letters* **1998,** *288* (2-4), 299-306.
43. Shiozaki, T.; Győrffy, W.; Celani, P.; Werner, H.-J., Communication: Extended multi-state complete active space second-order perturbation theory: Energy and nuclear gradients. *The Journal of Chemical Physics* **2011,** *135* (8).
44. Battaglia, S.; Lindh, R., Extended dynamically weighted CASPT2: The best of two worlds. *Journal of chemical theory and computation* **2020,** *16* (3), 1555-1567.
45. Granovsky, A. A., Extended multi-configuration quasi-degenerate perturbation theory: The new approach to multi-state multi-reference perturbation theory. *The Journal of chemical physics* **2011,** *134* (21).
46. Li Manni, G.; Carlson, R. K.; Luo, S.; Ma, D.; Olsen, J.; Truhlar, D. G.; Gagliardi, L., Multiconfiguration pair-density functional theory. *Journal of chemical theory and computation* **2014,** *10* (9), 3669-3680.
47. Gagliardi, L.; Truhlar, D. G.; Li Manni, G.; Carlson, R. K.; Hoyer, C. E.; Bao, J. L., Multiconfiguration pair-density functional theory: A new way to treat strongly correlated systems. *Accounts of chemical research* **2017,** *50* (1), 66-73.
48. Sharma, P.; Bao, J. J.; Truhlar, D. G.; Gagliardi, L., Multiconfiguration pair-density functional theory. *Annual review of physical chemistry* **2021,** *72*, 541-564.
49. Zhou, C.; Hermes, M. R.; Wu, D.; Bao, J. J.; Pandharkar, R.; King, D. S.; Zhang, D.; Scott, T. R.; Lykhin, A. O.; Gagliardi, L., Electronic structure of strongly correlated systems: recent developments in multiconfiguration pair-density functional theory and multiconfiguration nonclassical-energy functional theory. *Chemical Science* **2022,** *13* (26), 7685-7706.
50. Ai, Y.; Zhao, C.; Xing, J.; Liu, Y.; Wang, Z.; Jin, J.; Xia, S.; Cui, G.; Wang, X., Excited-state decay pathways of flavin molecules in five redox forms: the role of conical intersections. *The Journal of Physical Chemistry A* **2018,** *122* (40), 7954-7961.
51. Chang, X. P.; Gao, Y. J.; Fang, W. H.; Cui, G.; Thiel, W., Quantum mechanics/molecular mechanics study on the photoreactions of dark-and light-adapted states of a blue-light YtvA LOV photoreceptor. *Angewandte Chemie* **2017,** *129* (32), 9469-9473.
52. Climent, T.; González-Luque, R.; Merchán, M.; Serrano-Andrés, L., Theoretical insight into the spectroscopy and photochemistry of isoalloxazine, the flavin core ring. *The Journal of Physical Chemistry A* **2006,** *110* (50), 13584-13590.
53. Udvarhelyi, A.; Domratcheva, T., Photoreaction in BLUF receptors: proton-coupled electron transfer in the flavin-Gln-Tyr system. *Photochemistry and photobiology* **2011,** *87* (3), 554-563.
54. Khrenova, M.; Nemukhin, A. V.; Grigorenko, B. L.; Krylov, A.; Domratcheva, T., Quantum chemistry calculations provide support to the mechanism of the light-induced structural changes in the flavin-binding photoreceptor proteins. *Journal of Chemical Theory and Computation* **2010,** *6* (8), 2293-2302.
55. Udvarhelyi, A.; Olivucci, M.; Domratcheva, T., Role of the molecular environment in flavoprotein color and redox tuning: QM cluster versus QM/MM modeling. *Journal of Chemical Theory and Computation* **2015,** *11* (8), 3878-3894.

56. Khrenova, M. G.; Nemukhin, A. V.; Domratcheva, T., Theoretical characterization of the flavin-based fluorescent protein iLOV and its Q489K mutant. *The Journal of Physical Chemistry B* **2015,** *119* (16), 5176-5183.
57. Domratcheva, T., Neutral histidine and photoinduced electron transfer in DNA photolyases. *Journal of the American Chemical Society* **2011,** *133* (45), 18172-18182.
58. Luo, Y.; Liu, Y. J., Bioluminophore and flavin mononucleotide fluorescence quenching of bacterial bioluminescence—a theoretical study. *Chemistry–A European Journal* **2016,** *22* (45), 16243-16249.
59. Luo, Y.; Liu, Y.-J., Theoretical Insight into a Nonadiabatic Proton-Coupled Electron Transfer Mechanism of Reduced Flavin Oxygenation. *The Journal of Physical Chemistry A* **2019,** *123* (20), 4354-4359.
60. Zenichowski, K.; Gothe, M.; Saalfrank, P., Exciting flavins: Absorption spectra and spin–orbit coupling in light–oxygen–voltage (LOV) domains. *Journal of Photochemistry and Photobiology A: Chemistry* **2007,** *190* (2-3), 290-300.
61. Karasulu, B.; Götze, J. P.; Thiel, W., Assessment of Franck–Condon methods for computing vibrationally broadened UV–Vis absorption spectra of flavin derivatives: riboflavin, roseoflavin, and 5-thioflavin. *Journal of chemical theory and computation* **2014,** *10* (12), 5549-5566.
62. Goings, J. J.; Hammes-Schiffer, S., Early photocycle of Slr1694 blue-light using flavin photoreceptor unraveled through adiabatic excited-state quantum mechanical/molecular mechanical dynamics. *Journal of the American Chemical Society* **2019,** *141* (51), 20470-20479.
63. Mazzeo, P.; Hashem, S.; Lipparini, F.; Cupellini, L.; Mennucci, B., Fast method for excited-state dynamics in complex systems and its application to the photoactivation of a blue light using flavin photoreceptor. *The journal of physical chemistry letters* **2023,** *14* (5), 1222-1229.
64. Hou, C.; Liu, Y. J.; Ferré, N.; Fang, W. H., Understanding bacterial bioluminescence: a theoretical study of the entire process, from reduced flavin to light emission. *Chemistry–A European Journal* **2014,** *20* (26), 7979-7986.
65. Kowalczyk, M.; Sikorska, E.; Khmelinskii, I. V.; Komasa, J.; Insińska-Rak, M.; Sikorski, M., Spectroscopy and photophysics of flavin-related compounds: isoalloxazines. *Journal of Molecular Structure: THEOCHEM* **2005,** *756* (1-3), 47-54.
66. Giuliani, G.; Melaccio, F.; Gozem, S.; Cappelli, A.; Olivucci, M., QM/MM investigation of the spectroscopic properties of the fluorophore of bacterial luciferase. *Journal of chemical theory and computation* **2021,** *17* (2), 605-613.
67. Su, D.; Kabir, M. P.; Orozco-Gonzalez, Y.; Gozem, S.; Gadda, G., Fluorescence properties of flavin semiquinone radicals in nitronate monooxygenase. *ChemBioChem* **2019,** *20* (13), 1646-1652.
68. Orozco-Gonzalez, Y.; Kabir, M. P.; Gozem, S., Electrostatic spectral tuning maps for biological chromophores. *The Journal of Physical Chemistry B* **2019,** *123* (23), 4813-4824.
69. Dratch, B. D.; Orozco-Gonzalez, Y.; Gadda, G.; Gozem, S., Ionic atmosphere effect on the absorption spectrum of a flavoprotein: a reminder to consider solution ions. *The Journal of Physical Chemistry Letters* **2021,** *12* (34), 8384-8396.
70. Kabir, M. P.; Ouedraogo, D.; Orozco-Gonzalez, Y.; Gadda, G.; Gozem, S., Alternative strategy for spectral tuning of flavin-binding fluorescent proteins. *The Journal of Physical Chemistry B* **2023,** *127* (6), 1301-1311.
71. Jacoby Morris, K.; Barnard, D. T.; Narayanan, M.; Byrne, M. C.; McBride, R. A.; Singh, V. R.; Stanley, R. J., Comparing ultrafast excited state quenching of flavin 1, N 6-ethenoadenine dinucleotide and flavin adenine dinucleotide by optical spectroscopy and DFT calculations. *Photochemical & Photobiological Sciences* **2022,** *21* (6), 959-982.
72. Van Galen, C. J.; Pauszek, R. F.; Koder, R. L.; Stanley, R. J., Flavin Charge Redistribution upon Optical Excitation Is Independent of Solvent Polarity. *The Journal of Physical Chemistry B* **2023,** *127* (3), 661-672.
73. Pauszek III, R. F.; Kodali, G.; Siddiqui, M. S. U.; Stanley, R. J., Overlapping electronic states with nearly parallel transition dipole moments in reduced anionic flavin can distort photobiological dynamics. *Journal of the American Chemical Society* **2016,** *138* (45), 14880-14889.
74. Sayfutyarova, E. R.; Hammes-Schiffer, S., Constructing molecular π-orbital active spaces for multireference calculations of conjugated systems. *Journal of chemical theory and computation* **2019,** *15* (3), 1679-1689.
75. Dittrich, M.; Freddolino, P. L.; Schulten, K., When light falls in LOV: a quantum mechanical/molecular mechanical study of photoexcitation in Phot-LOV1 of Chlamydomonas reinhardtii. *The Journal of Physical Chemistry B* **2005,** *109* (26), 13006-13013.

76. Salzmann, S.; Tatchen, J.; Marian, C. M., The photophysics of flavins: What makes the difference between gas phase and aqueous solution? *Journal of Photochemistry and Photobiology A: Chemistry* **2008,** *198* (2-3), 221-231.
77. Salzmann, S.; Marian, C. M., The photophysics of alloxazine: a quantum chemical investigation in vacuum and solution. *Photochemical & Photobiological Sciences* **2009,** *8* (12), 1655-1666.
78. Kar, R. K.; Miller, A. F.; Mroginski, M. A., Understanding flavin electronic structure and spectra. *Wiley Interdisciplinary Reviews: Computational Molecular Science* **2022,** *12* (2), e1541.
79. Kar, R. K.; Borin, V. A.; Ding, Y.; Matysik, J.; Schapiro, I., Spectroscopic Properties of Lumiflavin: A Quantum Chemical Study. *Photochemistry and photobiology* **2019,** *95* (2), 662-674.
80. Rieff, B.; Bauer, S.; Mathias, G.; Tavan, P., DFT/MM description of flavin IR spectra in BLUF domains. *The Journal of Physical Chemistry B* **2011,** *115* (38), 11239-11253.
81. Wu, M.; Eriksson, L. A., Absorption Spectra of Riboflavin□ A Difficult Case for Computational Chemistry. *The Journal of Physical Chemistry A* **2010,** *114* (37), 10234-10242.
82. Sayfutyarova, E. R.; Sun, Q.; Chan, G. K.; Knizia, G., Automated Construction of Molecular Active Spaces from Atomic Valence Orbitals. *J Chem Theory Comput* **2017,** *13* (9), 4063-4078.
83. Bao, J. J.; Dong, S. S.; Gagliardi, L.; Truhlar, D. G., Automatic selection of an active space for calculating electronic excitation spectra by MS-CASPT2 or MC-PDFT. *Journal of Chemical Theory and Computation* **2018,** *14* (4), 2017-2025.
84. Jeong, W.; Stoneburner, S. J.; King, D.; Li, R.; Walker, A.; Lindh, R.; Gagliardi, L., Automation of Active Space Selection for Multireference Methods via Machine Learning on Chemical Bond Dissociation. *J Chem Theory Comput* **2020,** *16* (4), 2389-2399.
85. Kaufold, B. W.; Chintala, N.; Pandeya, P.; Dong, S. S., Automated Active Space Selection with Dipole Moments. *J Chem Theory Comput* **2023,** *19* (9), 2469-2483.
86. Stein, C. J.; Reiher, M., Automated selection of active orbital spaces. *Journal of chemical theory and computation* **2016,** *12* (4), 1760-1771.
87. Stanton, J. F.; Bartlett, R. J., The equation of motion coupled-cluster method. A systematic biorthogonal approach to molecular excitation energies, transition probabilities, and excited state properties. *The Journal of chemical physics* **1993,** *98* (9), 7029-7039.
88. Krylov, A. I., Equation-of-motion coupled-cluster methods for open-shell and electronically excited species: The hitchhiker's guide to Fock space. *Annu. Rev. Phys. Chem.* **2008,** *59*, 433-462.
89. Rhee, Y. M.; Head-Gordon, M., Scaled second-order perturbation corrections to configuration interaction singles: Efficient and reliable excitation energy methods. *The Journal of Physical Chemistry A* **2007,** *111* (24), 5314-5326.
90. Kao, Y.-T.; Saxena, C.; He, T.-F.; Guo, L.; Wang, L.; Sancar, A.; Zhong, D., Ultrafast dynamics of flavins in five redox states. *Journal of the American Chemical Society* **2008,** *130* (39), 13132-13139.
91. North, M. A.; Bhattacharyya, S.; Truhlar, D. G., Improved density functional description of the electrochemistry and structure− property descriptors of substituted flavins. *The Journal of Physical Chemistry B* **2010,** *114* (46), 14907-14915.
92. Kao, Y.-T.; Tan, C.; Song, S.-H.; Öztürk, N.; Li, J.; Wang, L.; Sancar, A.; Zhong, D., Ultrafast dynamics and anionic active states of the flavin cofactor in cryptochrome and photolyase. *Journal of the American Chemical Society* **2008,** *130* (24), 7695-7701.
93. Stein, C. J.; Pantazis, D. A.; Krewald, V., Orbital entanglement analysis of exchange-coupled systems. *The journal of physical chemistry letters* **2019,** *10* (21), 6762-6770.
94. Stein, C. J.; Reiher, M., autoCAS: A program for fully automated multiconfigurational calculations. *Journal of Computational Chemistry* **2019,** *40* (25), 2216-2226.
95. Forsberg, N.; Malmqvist, P.-Å., Multiconfiguration perturbation theory with imaginary level shift. *Chemical Physics Letters* **1997,** *274* (1-3), 196-204.
96. Roos, B. O.; Andersson, K., Multiconfigurational perturbation theory with level shift—the Cr2 potential revisited. *Chemical physics letters* **1995,** *245* (2-3), 215-223.
97. Roos, B. O.; Andersson, K.; Fülscher, M. P.; Serrano-Andrés, L.; Pierloot, K.; Merchán, M.; Molina, V., Applications of level shift corrected perturbation theory in electronic spectroscopy. *Journal of Molecular Structure: THEOCHEM* **1996,** *388*, 257-276.
98. Ghigo, G.; Roos, B. O.; Malmqvist, P.-Å., A modified definition of the zeroth-order Hamiltonian in multiconfigurational perturbation theory (CASPT2). *Chemical physics letters* **2004,** *396* (1-3), 142-149.
99. Zobel, J. P.; Nogueira, J. J.; Gonzalez, L., The IPEA dilemma in CASPT2. *Chem Sci* **2017,** *8* (2), 1482-1499.

100. Becke, A. D., Density-functional exchange-energy approximation with correct asymptotic behavior. *Physical review A* **1988,** *38* (6), 3098.
101. Lee, C.; Yang, W.; Parr, R. G., Development of the Colle-Salvetti correlation-energy formula into a functional of the electron density. *Physical review B* **1988,** *37* (2), 785.
102. Yanai, T.; Tew, D. P.; Handy, N. C., A new hybrid exchange–correlation functional using the Coulomb-attenuating method (CAM-B3LYP). *Chemical physics letters* **2004,** *393* (1-3), 51-57.
103. Chai, J.-D.; Head-Gordon, M., Long-range corrected hybrid density functionals with damped atom–atom dispersion corrections. *Physical Chemistry Chemical Physics* **2008,** *10* (44), 6615-6620.
104. Frisch, M. e.; Trucks, G.; Schlegel, H.; Scuseria, G.; Robb, M.; Cheeseman, J.; Scalmani, G.; Barone, V.; Petersson, G.; Nakatsuji, H., Gaussian 16. Gaussian, Inc. Wallingford, CT: 2016.
105. Fdez. Galván, I.; Vacher, M.; Alavi, A.; Angeli, C.; Aquilante, F.; Autschbach, J.; Bao, J. J.; Bokarev, S. I.; Bogdanov, N. A.; Carlson, R. K., OpenMolcas: From source code to insight. *Journal of chemical theory and computation* **2019,** *15* (11), 5925-5964.
106. Keller, S.; Dolfi, M.; Troyer, M.; Reiher, M., An efficient matrix product operator representation of the quantum chemical Hamiltonian. *The Journal of chemical physics* **2015,** *143* (24), 244118.
107. Shao, Y.; Gan, Z.; Epifanovsky, E.; Gilbert, A. T.; Wormit, M.; Kussmann, J.; Lange, A. W.; Behn, A.; Deng, J.; Feng, X., Advances in molecular quantum chemistry contained in the Q-Chem 4 program package. *Molecular Physics* **2015,** *113* (2), 184-215.
108. Bayliss, N. S.; McRae, E. G., Solvent effects in organic spectra: dipole forces and the Franck–Condon principle. *The Journal of Physical Chemistry* **1954,** *58* (11), 1002-1006.
109. Losi, A.; Gärtner, W., Old chromophores, new photoactivation paradigms, trendy applications: flavins in blue light-sensing photoreceptors. *Photochemistry and photobiology* **2011,** *87* (3), 491-510.
110. Losi, A.; Gärtner, W., The evolution of flavin-binding photoreceptors: an ancient chromophore serving trendy blue-light sensors. *Annual review of plant biology* **2012,** *63*, 49-72.
111. Christie, J. M.; Gawthorne, J.; Young, G.; Fraser, N. J.; Roe, A. J., LOV to BLUF: flavoprotein contributions to the optogenetic toolkit. *Molecular plant* **2012,** *5* (3), 533-544.
112. Conrad, K. S.; Manahan, C. C.; Crane, B. R., Photochemistry of flavoprotein light sensors. *Nature chemical biology* **2014,** *10* (10), 801-809.
113. Srivastava, V.; Singh, P. K.; Srivastava, A.; Singh, P. P., Synthetic applications of flavin photocatalysis: a review. *RSC Advances* **2021,** *11* (23), 14251-14259.
114. König, B.; Kümmel, S.; Svobodová, E.; Cibulka, R., Flavin photocatalysis. *Physical Sciences Reviews* **2018,** *3* (8), 20170168.
115. Cibulka, R., Artificial flavin systems for chemoselective and stereoselective oxidations. *European Journal of Organic Chemistry* **2015,** *2015* (5), 915-932.
116. Gozem, S.; Huntress, M.; Schapiro, I.; Lindh, R.; Granovsky, A. A.; Angeli, C.; Olivucci, M., Dynamic Electron Correlation Effects on the Ground State Potential Energy Surface of a Retinal Chromophore Model. *J Chem Theory Comput* **2012,** *8* (11), 4069-80.
117. Gozem, S.; Melaccio, F.; Lindh, R.; Krylov, A. I.; Granovsky, A. A.; Angeli, C.; Olivucci, M., Mapping the Excited State Potential Energy Surface of a Retinal Chromophore Model with Multireference and Equation-of-Motion Coupled-Cluster Methods. *J Chem Theory Comput* **2013,** *9* (10), 4495-506.
118. Gozem, S.; Krylov, A. I.; Olivucci, M., Conical Intersection and Potential Energy Surface Features of a Model Retinal Chromophore: Comparison of EOM-CC and Multireference Methods. *J Chem Theory Comput* **2013,** *9* (1), 284-92.
119. Gozem, S.; Melaccio, F.; Valentini, A.; Filatov, M.; Huix-Rotllant, M.; Ferre, N.; Frutos, L. M.; Angeli, C.; Krylov, A. I.; Granovsky, A. A., Shape of multireference, equation-of-motion coupled-cluster, and density functional theory potential energy surfaces at a conical intersection. *Journal of chemical theory and computation* **2014,** *10* (8), 3074-3084.
120. Huix-Rotllant, M.; Filatov, M.; Gozem, S.; Schapiro, I.; Olivucci, M.; Ferre, N., Assessment of Density Functional Theory for Describing the Correlation Effects on the Ground and Excited State Potential Energy Surfaces of a Retinal Chromophore Model. *J Chem Theory Comput* **2013,** *9* (9), 3917-32.
121. Xu, X.; Gozem, S.; Olivucci, M.; Truhlar, D. G., Combined Self-Consistent-Field and Spin-Flip Tamm-Dancoff Density Functional Approach to Potential Energy Surfaces for Photochemistry. *J Phys Chem Lett* **2013,** *4* (2), 253-8.
122. Zen, A.; Coccia, E.; Gozem, S.; Olivucci, M.; Guidoni, L., Quantum Monte Carlo Treatment of the Charge Transfer and Diradical Electronic Character in a Retinal Chromophore Minimal Model. *J Chem Theory Comput* **2015,** *11* (3), 992-1005.

123. Tuna, D.; Lefrancois, D.; Wolański, Ł.; Gozem, S.; Schapiro, I.; Andruniów, T.; Dreuw, A.; Olivucci, M., Assessment of approximate coupled-cluster and algebraic-diagrammatic-construction methods for ground-and excited-state reaction paths and the conical-intersection seam of a retinal-chromophore model. *Journal of Chemical Theory and Computation* **2015,** *11* (12), 5758-5781.
124. Gozem, S.; Luk, H. L.; Schapiro, I.; Olivucci, M., Theory and simulation of the ultrafast double-bond isomerization of biological chromophores. *Chemical reviews* **2017,** *117* (22), 13502-13565.
125. Marsili, E.; Farag, M. H.; Yang, X.; De Vico, L.; Olivucci, M., Two-State, Three-Mode Parametrization of the Force Field of a Retinal Chromophore Model. *J Phys Chem A* **2019,** *123* (9), 1710-1719.

Graphical Abstract